SCIENTIFIC REPORTS

OPEN

SUBJECT AREAS:
NANOSCALE MATERIALS
MATERIALS FOR ENERGY AND CATALYSIS
ELECTROCHEMISTRY
MATERIALS CHEMISTRY

Received
17 December 2012

Accepted
4 March 2013

Published
18 March 2013

Correspondence and requests for materials should be addressed to X.W.L. (xwlou@ntu.edu.sg)

# Controlled Growth of $NiCo_2O_4$ Nanorods and Ultrathin Nanosheets on Carbon Nanofibers for High-performance Supercapacitors

Genqiang Zhang[1,2] & Xiong Wen (David) Lou[1,2]

[1]TUM-CREATE Centre for Electromobility, 62 Nanyang Drive, Singapore, 637459, [2]School of Chemical and Biomedical Engineering, Nanyang Technological University, 62 Nanyang Drive, Singapore, 637459.

**Two one-dimensional hierarchical hybrid nanostructures composed of $NiCo_2O_4$ nanorods and ultrathin nanosheets on carbon nanofibers (CNFs) are controllably synthesized through facile solution methods combined with a simple thermal treatment. The structure of $NiCo_2O_4$ can be easily controlled to be nanorods or nanosheets by using different additives in the synthesis. These two different nanostructures are evaluated as electrodes for high performance supercapacitors, in view of their apparent advantages, such as high electroactive surface area, ultrathin and porous features, robust mechanical strength, shorter ion and electron transport path. Their electrochemical performance is systematically studied, and both of these two hierarchical hybrid nanostructures exhibit high capacitance and excellent cycling stability. The remarkable electrochemical performance will undoubtedly make these hybrid structures attractive for high-performance supercapacitors with high power and energy densities.**

In recent years, the research on supercapacitors (SCs) has been intensely stimulated due to their advantages of higher power density, faster charge/discharge process and longer lifespan, which make them attractive as power resources in high power electric devices and electric vehicles[1–4]. Despite the significant advances achieved in electrode materials for SCs[5–10], the practical applications of supercapacitors are still seriously hindered due to the relatively poor performance of the electrode materials, such as low specific capacitance in carbon based materials, poor cycling stability in transition metal oxides, and very high cost of $RuO_2$ based materials. Therefore, more efforts are still desired to further improve the electrochemical performance of electrode materials in order to build better SCs with both high power and energy densities. It has been proven to be an effective strategy that nanostructure engineering, including nanoparticles, hollow nano-architectures and one-dimensional (1D) nanostructures could greatly contribute to the optimization of electrode properties with higher capacity/capacitance because of the increased active surface areas, short ion transport pathways and so on[11–16]. Nevertheless, the fast fading of capacitance is still a common drawback in various nanostructured electrode materials when applied as electrodes in SCs.

Recently, an emerging concept of 1D hybrid nanostructures, such as nanocables, ordered nanostructure/carbon nanotube and graphene as well as hybrid nanowire/nanotube arrays, has been demonstrated as a promising solution to fabricate energy storage devices with high capacity/capacitance, good cycling stability and rate performance[17–27]. As an example, Ajayan and coworkers synthesized CNT@$MnO_2$ nanocables through a template-assisted electrodeposition method and successfully enhanced both the capacity and cycling performance when served as anode materials in lithium-ion batteries (LIBs)[28]. However, current research on hybrid nanostructures mainly focuses on the simple binary metal oxide materials perhaps due to the lack of available synthesis methods for complex multi-component metal oxides. This will undoubtedly limit the exploitation of high-performance electrode materials since it has been broadly demonstrated that the synergistic effect in complex metal oxides could further improve the performance in energy storage applications. Therefore, it will be of great significance to develop facile and simple methods suitable for building complex oxides based 1D hierarchical hybrid nanostructures.

As one of the most promising candidates, ternary nickel cobaltite ($NiCo_2O_4$) has recently been investigated as a high-performance electrode material for SCs since it possesses better electrical conductivity and electrochemical

activity compared to those of binary nickel oxide (NiO) and cobalt oxide ($Co_3O_4$). Several different types of $NiCo_2O_4$ nanostructures have been recently synthesized and their electrochemical performance is investigated. For example, Lu and coworkers fabricated $NiCo_2O_4$ nanoparticles using an epoxide-assisted sol-gel method and a largely enhanced capacitance is achieved[29]. In addition, $NiCo_2O_4$ nanowires have also been obtained through polymer/surfactant-assisted hydrothermal or solution methods, exhibiting both high capacitance and good cycling ability[30,31]. Recently, we developed a facile solution method to grow $NiCo_2O_4$ mesoporous nanosheets on various conductive substrates as integrated electrodes for supercapacitors[32]. However, to the best of our knowledge, the synthesis of $NiCo_2O_4$ 1D hierarchical nanostructures composed of nanorod arrays or ultrathin nanosheets remains unreported till now.

## Results

In this work, we successfully developed a facile low-temperature solution method combined with a simple post annealing process for controllable synthesis of 1D hierarchical hybrid nanostructures composed of $NiCo_2O_4$ nanorods or ultrathin nanosheets grown on carbon nanofibers (CNFs), denoted as CNF@$NiCo_2O_4$ NR and CNF@$NiCo_2O_4$ NS, respectively. The CNFs are synthesized through a modified Te-nanowire template directed hydrothermal method[33,34]. The typical transmission electron microscope (TEM) images of the as-synthesized and Te-nanowire core removed CNFs clearly indicate the purity of CNFs (Fig. S1, see the Supporting Information). Typical field-emission scanning electron microscope (FESEM) images of CNFs (Fig. 1A, B) indicate the large-scale and uniform features of the products. The average diameter of the CNFs is in the range of 220–280 nm, and the length can reach tens of micrometers. The X-ray diffraction (XRD) pattern (Fig. S2A, see the Supporting Information) indicates the typical amorphous feature of the CNFs. In addition, no peak from the Te phase is detected, indicating that the Te nanowires core template is completely removed through the $H_2O_2$/HCl/$H_2O$ mixed solution etching. It should be noted that the controlled synthesis of CNFs with a relatively large diameter will be important for the subsequent growth process since good mechanical robustness will be required in order to form well defined hierarchical structures. When urea is used to adjust the pH value, well defined NiCo-precursor nanorod arrays can be grown on CNFs (See Experimental section for detailed the synthesis procedure), which can be easily converted to CNF@$NiCo_2O_4$4 NR structure through annealing in air. Fig. 1C–F shows the typical FESEM images of the NiCo-precursor and the crystallized CNF@$NiCo_2O_4$ NR hybrid structure. As can be seen, the NiCo-precursor nanorods (Fig. 1C, D, Fig. S3A in the Supporting Information) can be uniformly grown on the CNFs to form a large-scale conformal coating. In addition, the nanorods exhibit a hierarchical array feature with empty space among adjacent nanorods. This feature could benefit the penetration of the electrolyte, which may contribute to the optimization of electrochemical performance. The corresponding XRD pattern (Fig. S2B, see the Supporting Information) of NiCo-precursor nanorods is similar to that of the cobalt nickel carbonate hydroxide hydrate (JCPDS card no. 40-0216). After annealing, the NiCo-precursor nanorods can be converted to crystallized $NiCo_2O_4$ nanorods and the corresponding XRD pattern (Fig. S2C) can be readily indexed to the cubic $NiCo_2O_4$ phase (JCPDS card no. 20-0781). As shown in Fig. 1E, F (also Fig. S3B, see the Supporting Information), both the nanorod morphology and the array feature of the nanorods are perfectly retained after the annealing conversion, which could be derived from the robust support of CNFs with a relatively large diameter, as well as the slow heating rate applied during the annealing. The energy-dispersive X-ray spectroscopy (EDS) measurement (Fig. S4, see the Supporting Information) shows that the molar ratio of Ni to Co is almost 1 : 2, which further confirms formation of the $NiCo_2O_4$ phase. The mass content of the $NiCo_2O_4$ nanorods in the hybrid structure is estimated by the thermogravimetric analysis (TGA) (Fig. S5, see the Supporting Information), which shows that the mass fraction of $NiCo_2O_4$ is as high as 92% in the hybrid nanostructure. Fig. 2 gives the typical TEM images of the CNF@$NiCo_2O_4$ NR hybrid structure. The low-magnification image (Fig. 2A) demonstrates the uniform growth of $NiCo_2O_4$ nanorods surrounding the CNFs backbone. An enlarged view (Fig. 2B) provides the evidence that the $NiCo_2O_4$ nanorods are chemically grown on the carbon nanofibers, which could be derived from the self-seeded growth process[35]. In addition, it could be observed that the nanorods possess a needle-like shape with a sharp tip. The length of the nanorods could be estimated to be around 400 nm while the diameter of the nanorods ranges from several nanometers at the tips to around 20 nm near the bottom of the nanorods (Fig. 2C). The inset in Fig. 2C gives the selected-area electron diffraction (SAED) pattern, indicating the crystalline nature of the nanorods. As described above, the well defined CNF@$NiCo_2O_4$ NR hybrid nanostructure can be obtained by this low-cost effective solution route.

By simply replacing the urea with hexamethylenetetramine during the synthesis, ultrathin nanosheets of NiCo-precursor can be grown

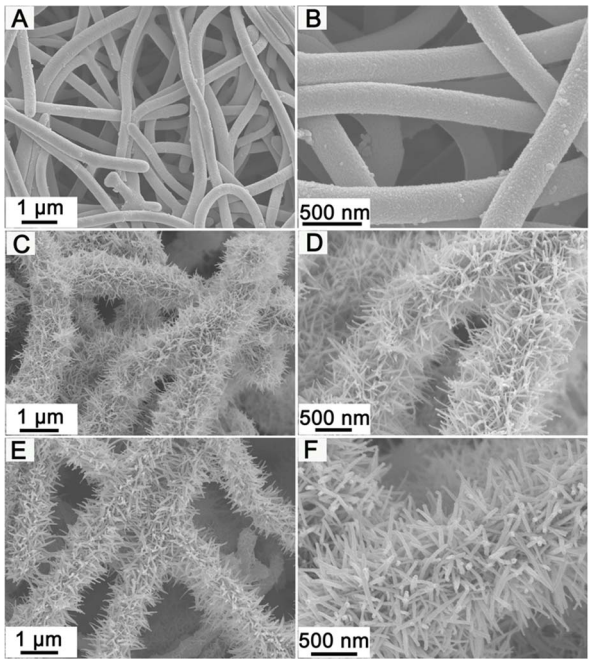


**Figure 1 | Typical FESEM images of (A, B) bare carbon nanofibers after Te nanowire core removal; (C, D) NiCo-precursor nanorod arrays/carbon nanofibers hybrid nanostructure; and (E, F) crystalline $NiCo_2O_4$ nanorod arrays/carbon nanofibers hybrid structure obtained by annealing the NiCo-precursor nanorods/carbon nanofibers at 300°C for 2 h with a slow heating rate of 0.5°C $min^{-1}$.**

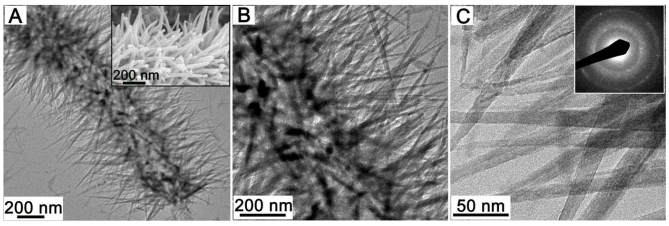


**Figure 2 | Typical TEM images of crystalline $NiCo_2O_4$ nanorod arrays/carbon nanofibers hybrid nanostructure.** The inset in (A) is an enlarged view of corresponding FESEM image, and the inset in (C) is the corresponding SAED pattern.

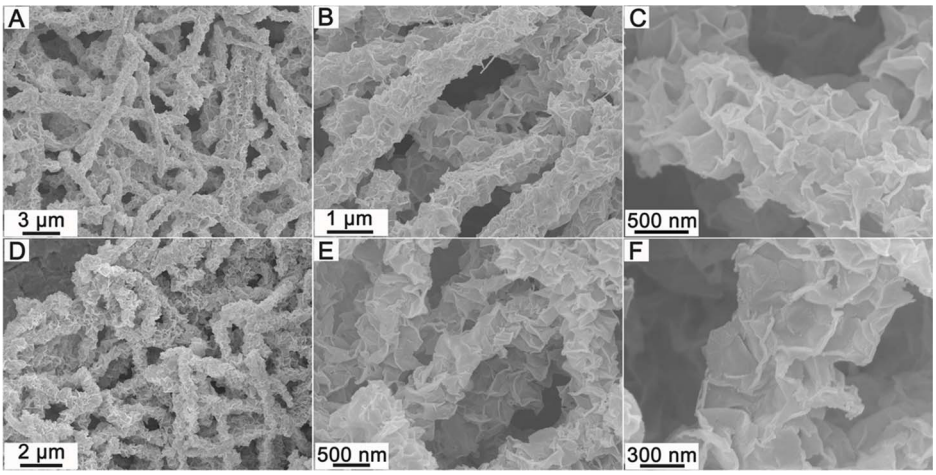


**Figure 3 | Typical FESEM images at different magnifications of (A–C) CNF@NiCo-precursor ultrathin nanosheets hierarchical nanostructures, and (D–F) CNF@$NiCo_2O_4$ NS hybrid nanostructure after annealing at 350°C for 2 h in air with a heating rate of 1°C $min^{-1}$.**

on CNFs with a conformal coating. As can be seen in Fig. 3A, large amount of uniform 1D nanostructures can be obtained with a hierarchical architecture compared to that of bare CNFs shown in Fig. 1A. From an enlarged view of the FESEM images (Fig. 3B, C), these 1D nanostructures are composed of uniform and ultrathin nanosheets grown surrounding the surface of CNFs. After annealing, the NiCo-precursor nanosheets can be fully converted to crystallized $NiCo_2O_4$ nanosheets and the corresponding XRD pattern (Fig. S6, see the Supporting Information) can be readily indexed to the cubic $NiCo_2O_4$ phase (JCPDS card no. 20-0781). The ultrathin nanosheet morphology (Fig. 3 D–F) is well retained after the annealing conversion, which could also benefit from the robust support of CNFs with a relatively large diameter. Fig. 4 shows the corresponding TEM images of the CNF@NiCo-precursor and CNF@$NiCo_2O_4$ NS hierarchical nanostructures. It can be clearly observed (Fig. 4A, B) that ultrathin NiCo-precursor nanosheets are grown uniformly on the CNFs to form the 1D structure. In addition, the thickness of the nanosheets could be ultrathin from the contrast in the TEM image (Fig. 4B). TEM images of the CNF@$NiCo_2O_4$ NS (Fig. 4C, D) reveal that the ultrathin nanosheet morphology of the NiCo-precursor is well retained after the thermal conversion. However, the CNF core is largely burned away during the annealing in air at 350°C. The content of the CNFs in the hybrid structure estimated by TGA analysis (Fig. S7, see the Supporting Information) is only around 5.7 wt.%. Interestingly, a magnified view of the crystalline $NiCo_2O_4$ nanosheets (Fig. 4E) clearly indicates the porous feature of the ultrathin nanosheets. The SAED pattern (Fig. 4F) indicates the polycrystalline nature of the $NiCo_2O_4$ nanosheets and can be readily indexed to (200), (311), (400), (420) and (440) crystal planes of the cubic $NiCo_2O_4$ phase, which is consistent with the XRD characterization. It is worth to mention that both the ultrathin and porous features of the $NiCo_2O_4$ nanosheets could contribute to the optimization of the electrochemical performance, which will be discussed shortly.

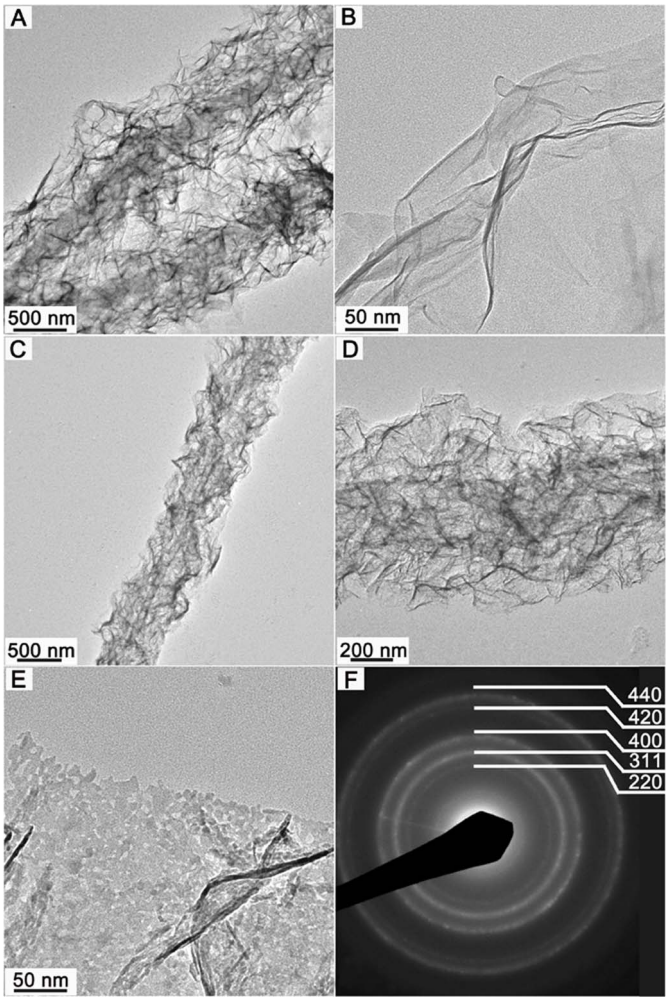


**Figure 4 | TEM images of (A, B) CNF@NiCo-precursor ultrathin nanosheets hierarchical nanostructures; (C, D) CNF@$NiCo_2O_4$ NS hybrid nanostructures after annealing at 350°C for 2 h in air with a heating rate of 1°C $min^{-1}$; (E) An enlarged view of the $NiCo_2O_4$ nanosheets revealing the mesoporous feature; (F) SAED pattern of the CNF@$NiCo_2O_4$ NS hybrid nanostructures.**

## Discussion

As described above, two different nanostructures of nanorods and ultrathin nanosheets can be controllably grown on CNFs by the developed simple solution methods followed by a thermal annealing treatment. It will be interesting to study the electrochemical performance of these two different hybrid nanostructures consisting of the same active material. First, the electrochemical performance of the CNF@$NiCo_2O_4$ NR hybrid structure is studied as electrodes for SCs. Fig. 5A shows the typical cyclic voltammetry (CV) curves of the CNF@$NiCo_2O_4$ NR nanostructure electrode with various sweep rates ranging from 2 to 60 mV $s^{-1}$. The shape of the CV curves clearly

reveals the pseudocapacitive characteristics. Specifically, a pair of redox peaks can be observed within the potential range from 0 to 0.6 V vs. SCE for all sweep rates, which is mainly associated with the Faradaic redox reactions related to M-O/M-O-OH, where M refers to Ni or Co[36]. Fig. 5B shows the constant current discharge profiles at different current densities. It can be observed that there are voltage plateaus at around 0.3 V, which is consistent with the CV curves. The specific capacitance is calculated by the formula, $C = I\Delta t/m\Delta V$, where I is the discharge current, $\Delta t$ is the discharge time, $\Delta V$ is the voltage range and m is the mass of the active material (i.e., the total mass of the hybrid nanostructure). The calculated specific capacitance as a function of the discharge current density is plotted in Fig. 5C. Notably, the specific capacitance is as high as 1023.6, 888.7, 728, 656, 630, 500 F $g^{-1}$ at the discharge current densities of 1, 2, 4, 8, 10 and 20 A $g^{-1}$, respectively. In addition, the cycling stability is also evaluated by the repeated charging-discharging measurement at a constant current density of 2 A $g^{-1}$, as shown in Fig. 5D. The specific capacitance is around 888.7 F $g^{-1}$ in the first cycle and it gradually decreases to 810.8 F $g^{-1}$ after cycling for 2000 times. This corresponds to a capacitance loss of only 8.5%, which is considered very good for metal oxide nanostructures based electrode materials. The improved electrochemical performance could be related to the following structural features. First, the well-defined nanorods array feature leads to the separation of neighboring nanorods from each other and makes most surface of nanorods effectively accessible by electrolyte. This will give high capacitance and enhanced electrochemical kinetics relative to conventional film electrodes and free-standing nanowires. Second, the CNFs provide a robust support for the $NiCo_2O_4$ nanorods, which could ensure good mechanical adhesion and better cycling stability. Third, the relatively small diameter of the $NiCo_2O_4$ nanorods could facilitate the ion transport for the charge and discharge processes, which may also contribute to the enhancement of specific capacitance at high current densities.

Next, the electrochemical performance of the CNF@$NiCo_2O_4$ NS hybrid nanostructure is evaluated as electrodes for SCs. Fig. 6A shows the typical CV curves of the CNF@$NiCo_2O_4$ NS hybrid nanostructure electrode with various sweep rates ranging from 5 to 80 mV $s^{-1}$. Similarly, the shape of the CV curves clearly reveals the pseudocapacitive characteristics. A pair of redox peaks can be observed within the potential range from 0 to 0.65 V vs. SCE at all sweep rates, which is mainly associated with the Faradaic redox reactions related to M-O/M-O-OH, where M refers to Ni or Co[36]. Fig. 6B shows the constant current charge/discharge profiles at different current densities. The calculated specific capacitance as a function of the discharge current density is plotted in Fig. 6C. Notably, the specific capacitance is as high as 1002, 905, 828, 725, 675 and 520 F $g^{-1}$ at the discharge current densities of 1, 2, 4, 8, 10 and 20 A $g^{-1}$, respectively. In addition, the cycling stability is also evaluated by the repeated charging-discharging measurement at constant current densities of 2 and 5 A $g^{-1}$, as shown in Fig. 6D. At the discharge current density of 2 A $g^{-1}$, the specific capacitance is around 905 F $g^{-1}$ in the first cycle, and it slightly increases to 942 F $g^{-1}$ in the course of first four hundred cycles. After that, it gradually decreases to 872 F $g^{-1}$ after 2400 cycles, resulting in an overall capacitance loss of only 3.6%. Even at a higher discharge current density of 5 A $g^{-1}$, the specific capacitance can reach 737 F $g^{-1}$ in the first cycle and gradually decreases to 684 F $g^{-1}$ after 2400 cycles. This corresponds to a capacitance loss of 7.25%, which is still remarkable considering the relatively high discharge current density.

The electrochemical measurement indicates that the CNF@$NiCo_2O_4$ NS hybrid nansotructure delivers remarkable specific capacitance with excellent cycling stability. The superior electrochemical performance could be derived from the following structural features. First, the ultrathin feature of the $NiCo_2O_4$ nanosheets will facilitate the electrolyte ion and electron transport. Second, the porous feature of the $NiCo_2O_4$ nanosheets largely increases the amount of electroactive sites. Third, the 1D hierarchical nanostructure composed of these ultrathin porous nanosheets on CNFs backbone could facilitate the electron transfer, and the electrolyte penetration. In addition, the CNFs backbone will provide better mechanical integrity, which could

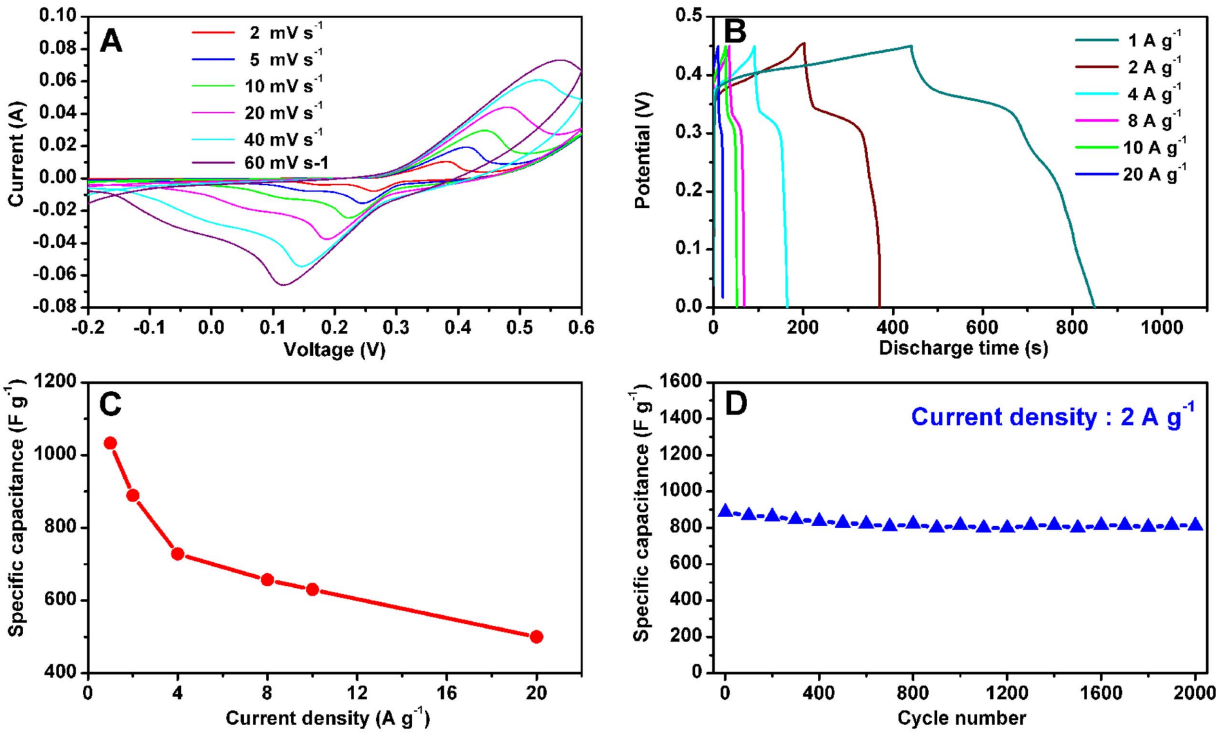


**Figure 5 | Electrochemical characterizations of the CNF@$NiCo_2O_4$ NR hybrid nanostructure.** (A) CV curves at various scan rates ranging from 2 to 60 mV $s^{-1}$; (B) Discharge voltage profiles at various current densities ranging from 1 to 20 A $g^{-1}$; (C) The capacitance as a function of current density; (D) The capacitance cycling performance at a constant current density of 2 A $g^{-1}$.

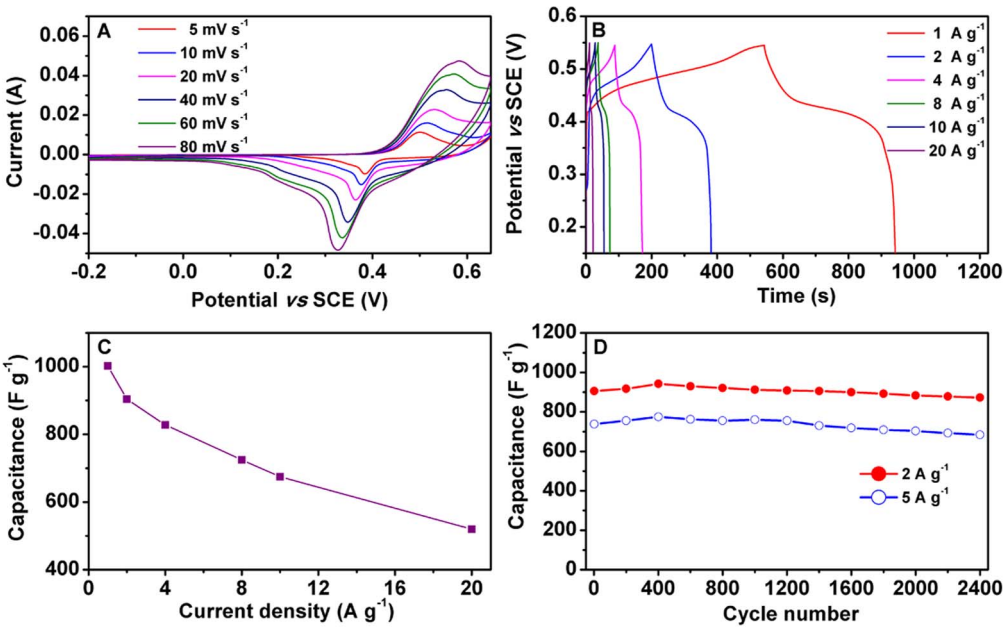


**Figure 6 | Electrochemical characterizations of the CNF@$NiCo_2O_4$ NS hybrid nanostructure.** (A) CV curves at various scan rates ranging from 5 to 80 mV $s^{-1}$; (B) Charge/discharge voltage profiles at various current densities ranging from 1 to 20 A $g^{-1}$; (C) The calculated capacitance as a function of current density according to the data in (B); (D) The capacitance cycling performance at constant current densities of 2 and 5 A $g^{-1}$.

sustain large structual alteration during the repeated charge/discharge processes. Compared to the CNF@$NiCo_2O_4$ NR structure, it can be clearly seen that the CNF@$NiCo_2O_4$ NS sample exhibits better supercapacitive performance with both higher capacitance and much better cycling stability. This might be understood by considering the following factors. First, the CNF@$NiCo_2O_4$ NS structure has a higher specific surface area, which is determined to be as high as 142.6 $m^2$ $g^{-1}$ by Brunauer-Emmett-Teller (BET) characterization compared to 104.2 $m^2$ $g^{-1}$ for the CNF@$NiCo_2O_4$ NR sample (Fig. S8, see the Supporting Information). In addition, there is a wide pore size distribution for the CNF@$NiCo_2O_4$ NS sample (Inset in Fig. S8B, see the Supporting Information) verifying the porous structure of the nanosheets, which is consistent with TEM results. The ultrathin nanosheet morphology is advantageous for efficient ion and electron transport since the thickness of the nanosheets is much smaller than the diameter of the nanorods, and for better accommodating the volume variation[4,37]. These will undoubtedly contribute to the enahncement of capacitance. The impedance of these two different hybrid structures appears similar (Fig. S9, see the Supporting Information).

In summary, two one-dimensional hybrid nanostructures composed of $NiCo_2O_4$ nanorod arrays and ultrathin porous nanosheets grown on carbon nanofibers are successfully fabricated through facile solution methods combined with a post annealing treatment. The electrochemical properties of these two hybrid nanostructures are evaluated as electrode materials for supercapacitors. It is found that the CNF@$NiCo_2O_4$ nanosheet hybrid nanostructure exhibits higher capacitance and much better cycling stability compared to CNF@$NiCo_2O_4$ nanorod structure. A high capacitance of 902 F $g^{-1}$ can be obtained for the CNF@$NiCo_2O_4$ nanosheet sample at a current density of 2 A $g^{-1}$ with a low capacitance loss of only 3.6% after 2400 cycles. This enhanced performance is attributed to several important structural factors of the CNF@$NiCo_2O_4$ nanosheet hybrid structure, including ultrathin and porous nanosheets, CNF support, and porous hierarchical structure. In view of the excellent electrochemical performance and the facile and cost-effective synthesis, these CNF@$NiCo_2O_4$ hierarchical hybrid nanostructures might hold great promise as advanced electrode materials for high-performance supercapacitors.

## Methods

**The synthesis of carbon nanofibers.** The carbon nanofibers are synthesized through a simple hydrothermal method using Te nanowire as the template. Firstly, 0.25 mmol of $TeO_2$ powder, 0.2 g of polyvinyl pyrrolidone (PVP; MW ~ 58000) and 10 mmol of NaOH are dissolved into 16 mL of ethylene glycol by heating to form a clear solution, which is then transferred into a 20 mL Teflon-lined autoclave. The Te nanowires are obtained after reaction at 180°C for 4 h. The obtained Te nanowires are washed with deionized (DI) water and ethanol for several times, which are then redispersed into 16 mL of DI water by sonication. Then, 5 mmol of glucose are added to the Te nanowire suspension solution, and the suspension is transferred into a 20 mL Teflon-lined autoclave after the glucose is dissolved. The autoclave is then heated at 180°C for 16 h to get the carbon nanofibers with Te nanowire cores. In order to remove the Te nanowires, the products are dispersed into $H_2O_2$/HCl/$H_2O$ mixed solution with a volume ratio of 2/5/23 for overnight. Pure carbon nanofibers can be obtained after washing with DI water and ethanol for several times.

**The synthesis of CNF@$NiCo_2O_4$ NR hybrid structure.** The obtained carbon nanofibers are re-dispersed into 50 mL of ethanol and sonicated for 30 min to reach good dispersion. 2 mmol of $Ni(NO_3)_2 \cdot 6H_2O$, 4 mmol of $Co(NO_3)_2 \cdot 6H_2O$ and 24 mmol of urea are dissolved into 50 mL of DI water to form a transparent pink solution. The above two solutions are then mixed and heated to 80°C in an oil bath for 6 h. After the solution is cooled down to room temperature naturally, the product is collected through centrifugation and washed with DI water and ethanol for several times. The products are then dried, followed by annealing at 300°C for 2 h with a slow heating rate of 0.5°C $min^{-1}$ in order to get well defined crystallized $NiCo_2O_4$ nanorod arrays/carbon nanofibers hybrid structure.

**The synthesis of CNF@$NiCo_2O_4$ NS hybrid nanostructures.** The obtained carbon nanofibers are re-dispersed into 20 mL of ethanol and sonicated for 30 min to reach good dispersion. 1 mmol of $Ni(NO_3)_2 \cdot 6H_2O$, 2 mmol of $Co(NO_3)_2 \cdot 6H_2O$ and 4.5 mmol of hexamethylenetetramine are dissolved into 40 mL of DI water to form a transparent pink solution. The above two solutions are then mixed and heated to 90°C in an oil bath for 4 h. After the solution is cooled down to room temperature naturally, the product is collected through centrifugation and washed with DI water and ethanol for several times. The products are then dried, followed by annealing at 350°C for 2 h with a slow heating rate of 1°C $min^{-1}$ in order to get CNF@$NiCo_2O_4$ NS hybrid nanostructures.

**Materials characterization.** X-ray diffraction (XRD) patterns were collected on a Bruker D8 Advanced X-Ray Diffractometer. Field-emission scanning electron microscope (FE-SEM) images were obtained on a JEOL JSM 6700F microscope. Transmission electron microscope (TEM) images were taken on a JEOL 2010 microscope. The nitrogen sorption measurement was performed on Autosorb 6B at −196°C. Thermogravimetric analysis (TGA) was carried out under air flow with a temperature ramp of 10°C $min^{-1}$.

**Electrochemical Measurements.** For electrochemical measurements, the working electrode is consisted of active material, carbon black (Super-P-Li), and polymer

binder (polyvinylidene fluoride; PVDF) in a weight ratio of 80 : 10 : 10. For supercapacitor test, the slurry was pasted to Ni foam and then dried at 120°C overnight under vacuum. The electrochemical tests were conducted with a CHI 660D electrochemical workstation in an aqueous KOH electrolyte (2.0 M) with a three-electrode cell where Pt foil serves as the counter electrode and a saturated calomel electrode (SCE) as the reference electrode. Electrochemical impedance spectroscopy (EIS) measurements were carried out by applying an AC voltage with 1 mV amplitude in a frequency range from 0.01 Hz to 100 kHz at open circuit potential.


1. Simon, P. & Gogotsi, Y. Materials for electrochemical capacitors. *Nat. Mater.* **7**, 845–854 (2008).
2. Miller, J. R. & Simon, P. Materials science - Electrochemical capacitors for energy management. *Science* **321**, 651–652 (2008).
3. Wei, W. Manganese oxide-based materials as electrochemical supercapacitor electrodes. *Chem. Soc. Rev.* **40**, 1697–1721 (2011).
4. Wang, G. P., Zhang, L. & Zhang, J. J. A review of electrode materials for electrochemical supercapacitors. *Chem. Soc. Rev.* **41**, 797–828 (2012).
5. Hall, P. J. *et al.* Energy storage in electrochemical capacitors: designing functional materials to improve performance. *Energy Environ. Sci.* **3**, 1238–1251 (2010).
6. Aricò, A. S. *et al.* Nanostructured materials for advanced energy conversion and storage devices. *Nat. Mater.* **4**, 366–377 (2005).
7. Yin, Z. G. & Zheng, Q. D. Controlled Synthesis and Energy Applications of One-Dimensional Conducting Polymer Nanostructures: An Overview. *Adv. Energy Mater.* **2**, 179–218 (2012).
8. Fang, Y. *et al.* Renewing Functionalized Graphene as Electrodes for High-Performance Supercapacitors. *Adv. Mater.* **47**, 6348–6355 (2012).
9. Zhang, L., Bin Wu, H. & Lou, X. W. Unusual $CoS_2$ ellipsoids with anisotropic tube-like cavities and their application in supercapacitors. *Chem. Commun.* **48**, 6912–6914 (2012).
10. Zhu, T., Chen, J. S. & Lou, X. W. Shape-controlled synthesis of porous $Co_3O_4$ nanostructures for application in supercapacitors. *J. Mater. Chem.* **20**, 7015–7020 (2010).
11. Poizot, P., Laruelle, S., Grugeon, S., Dupont, L. & Tarascon, J. M. Nano-sized transition-metaloxides as negative-electrode materials for lithium-ion batteries. *Nature* **407**, 496–499 (2000).
12. Lou, X. W., Archer, L. A. & Yang, Z. C. Hollow Micro-/Nanostructures: Synthesis and Applications. *Adv. Mater.* **20**, 3987–4019 (2008).
13. Lai, X. Y., Halpert, J. E. & Wang, D. Recent advances in micro-/nano-structured hollow spheres for energy applications: From simple to complex systems. *Energy Environ. Sci.* **5**, 5604–5618 (2012).
14. Lee, H.-W. *et al.* Ultrathin Spinel $LiMn_2O_4$ Nanowires as High Power Cathode Materials for Li-Ion Batteries. *Nano Lett.* **10**, 3852–3856 (2010).
15. Lee, K. T. & Cho, J. Roles of nanosize in lithium reactive nanomaterials for lithium ion batteries. *Nano Today* **6**, 28–41 (2011).
16. Arico, A. S., Bruce, P., Scrosati, B., Tarascon, J. M. & Van Schalkwijk, W. Nanostructured materials for advanced energy conversion and storage devices. *Nat. Mater.* 4, 366–377 (2005).
17. Cao, F. F., Guo, Y. G. & Wan, L. J. Better lithium-ion batteries with nanocable-like electrode materials. *Energy Environ. Sci.* **4**, 1634–1642 (2011).
18. Ding, S. J., Chen, J. S. & Lou, X. W. One-Dimensional Hierarchical Structures Composed of Novel Metal Oxide Nanosheets on a Carbon Nanotube Backbone and Their Lithium-Storage Properties. *Adv. Funct. Mater.* **21**, 4120–4125 (2011).
19. Wang, Z., Luan, D., Madhavi, S., Hu, Y. & Lou, X. W. Assembling carbon-coated alpha-$Fe_2O_3$ hollow nanohorns on the CNT backbone for superior lithium storage capability. *Energy Environ. Sci.* **5**, 5252–5256 (2012).
20. Mai, L.-Q. *et al.* Hierarchical $MnMoO_4/CoMoO_4$ heterostructured nanowires with enhanced supercapacitor performance. *Nat. Commun.* **2**, 381 (2011).
21. Luo, S. *et al.* Binder-Free $LiCoO_2$/Carbon Nanotube Cathodes for High-Performance Lithium Ion Batteries. *Adv. Mater.* 24, 2294–2298 (2012).
22. Liu, J. *et al.* $Co_3O_4$ Nanowire@$MnO_2$ Ultrathin Nanosheet Core/Shell Arrays: A New Class of High-Performance Pseudocapacitive Materials. *Adv. Mater.* **23**, 2076–2081 (2011).
23. Hu, L. B. *et al.* Symmetrical $MnO_2$-Carbon Nanotube-Textile Nanostructures for Wearable Pseudocapacitors with High Mass Loading. *ACS Nano* **5**, 8904–8913 (2011).
24. Chen, Z. *et al.* High-Performance Energy-Storage Architectures from Carbon Nanotubes and Nanocrystal Building Blocks. *Adv. Mater.* **24**, 2030–2036 (2012).
25. Ban, C. M. *et al.* Nanostructured $Fe_3O_4$/SWNT Electrode: Binder-Free and High-Rate Li-Ion Anode. *Adv. Mater.* **22**, E145–E149 (2010).
26. Qu, Q. 2D Sandwich-like Sheets of Iron Oxide Grown on Graphene as High Energy Anode Material for Supercapacitors. *Adv. Mater.* **23**, 5574 (2011).
27. Zhang, H. X. *et al.* Cross-Stacked Carbon Nanotube Sheets Uniformly Loaded with $SnO_2$ Nanoparticles: A Novel Binder-Free and High-Capacity Anode Material for Lithium-Ion Batteries. *Adv. Mater.* **21**, 2299–2304 (2009).
28. Reddy, A. L. M., Shaijumon, M. M., Gowda, S. R. & Ajayan, P. M. Coaxial $MnO_2$/Carbon Nanotube Array Electrodes for High-Performance Lithium Batteries. *Nano Lett.* **9**, 1002–1006 (2009).
29. Wei, T. Y., Chen, C. H., Chien, H. C., Lu, S. Y. & Hu, C. C. A Cost-Effective Supercapacitor Material of Ultrahigh Specific Capacitances: Spinel Nickel Cobaltite Aerogels from an Epoxide-Driven Sol-Gel Process. *Adv. Mater.* **22**, 347–351 (2010).
30. Wang, H. L., Gao, Q. M. & Jiang, L. Facile Approach to Prepare Nickel Cobaltite Nanowire Materials for Supercapacitors. *Small* **7**, 2454–2459 (2011).
31. Jiang, H., Ma, J. & Li, C. Z. Hierarchical porous $NiCo_2O_4$ nanowires for high-rate supercapacitors. *Chem. Commun.* **48**, 4465–4467 (2012).
32. Zhang, G. Q. & Lou, X. W. General Solution Growth of Mesoporous $NiCo_2O_4$ Nanosheets on Various Conductive Substrates as High-performance Electrodes for Supercapacitors. *Adv. Mater.* **25**, 976–979 (2013).
33. Liang, H. W. *et al.* Macroscopic-Scale Template Synthesis of Robust Carbonaceous Nanofiber Hydrogels and Aerogels and Their Applications. *Angew. Chem. Int. Ed.* **51**, 5101–5105 (2012).
34. Liang, H. W. *et al.* Highly Active Carbonaceous Nanofibers: A Versatile Scaffold for Constructing Multifunctional Free-Standing Membranes. *ACS Nano* **5**, 8148–8161 (2011).
35. Zhang, G. Q., Wu, H. B., Hoster, H. E., Chan-Park, M. B. & Lou, X. W. Single-crystalline $NiCo_2O_4$ Nanoneedle Arrays Grown on Conductive Substrates as Binder-free Electrodes for High-performance Supercapacitors. *Energy Environ. Sci.* **5**, 9453–9456 (2012).
36. Zhang, F. *et al.* Facile growth of mesoporous $Co_3O_4$ nanowire arrays on Ni foam for high performance electrochemical capacitors. *J. Power Sources* **203**, 250–256 (2012).
37. Cheng, F. *et al.* Facile Controlled Synthesis of $MnO_2$ Nanostructures of Novel Shapes and Their Application in Batteries. *Inorg. Chem.* **45**, 2038–2044 (2006).


## Acknowledgement

This publication is made possible with the financial support from the Singapore National Research Foundation under its Campus for Research Excellence and Technological Enterprise (CREATE) programme.

## Author contributions

G.Q. Zhang and X.W. Lou designed the experiment. G.Q. Zhang carried out the experiment. X.W. Lou and G.Q. Zhang carried out data analysis and co-wrote the manuscript.

## Additional information

**Supplementary information** accompanies this paper at http://www.nature.com/scientificreports

**Competing financial interests:** The authors declare no competing financial interests.



**How to cite this article:** Zhang, G.Q. & Lou, X. W. D. Controlled Growth of $NiCo_2O_4$ Nanorods and Ultrathin Nanosheets on Carbon Nanofibers for High-performance Supercapacitors. *Sci. Rep.* **3**, 1470; DOI:10.1038/srep01470 (2013).